Journal of Catalysis **190,** 387–395 (2000)
doi:10.1006/jcat.1999.2751, available online at http://www.idealibrary.com on IDEAL®

Behavior of Palladium–Copper Catalysts for CO and NO Elimination

M. Fernández-García,*,[1] A. Martínez-Arias,* C. Belver,* J. A. Anderson,† J. C. Conesa,* and J. Soria*

*Instituto de Catálisis, CSIC, Campus Cantoblanco, 28049 Madrid, Spain; and †Department of Chemistry, University of Dundee, Dundee DD1 4HN, Scotland, United Kingdom

Received August 2, 1999; revised November 1, 1999; accepted November 3, 1999

The behavior of a series of palladium and palladium–copper catalysts supported on ceria/alumina for the $CO + NO + O_2$ reaction has been analyzed by a combination of electron transmission microscopy, infrared, and electron paramagnetic spectroscopies and catalytic test studies. In both systems, the catalytic behavior is dominated by the properties of the metal–ceria interface. The addition of copper to a palladium system leads to beneficial effects related to alloy formation in which both CO and NO elimination are enhanced. The chemical consequences and catalytic implications of Pd-Cu alloying are discussed.

I. INTRODUCTION

The tightening of exhaust emission legislation expected for the XXI century will necessitate an improvement of current catalytic converter technology used in automobiles. Under stoichiometric conditions, low light-off catalysts, which start conversion of emitted gases at reduced operating temperatures, constitute one of the most successful ways to achieve this objective (1, 2). As lead is eliminated and sulfur levels in fuels are lowered, the use of palladium has increasingly attracted the attention of the catalytic community in order to develop efficient catalysts for hydrocarbon and CO oxidation at low temperatures (1, 3). The specific chemical-physical properties of the Pd–Ce interface have been determined as a result of studies concerning their catalytic behavior. For CO oxidation, contact between the metal and support yields surface metallic palladium from initial contact with the reactant gases at room temperature (RT) as well as creating surface ceria anion vacancies able to activate oxygen, which subsequently reacts with CO adsorbed on metallic sites to generate CO_2 (3). Both effects are characteristic of the Pd-Ce interaction, with a similar effect for other noble metals such as Pt only being observed at significantly higher temperatures (3, 4).

However, the performance of Pd-based systems for NO elimination usually requires improvements in order to reach acceptable standards of current systems (1, 2). Substitution of Rh in three-way catalysts (TWCs) is another desirable objective from an economical view, and promotion of Pd with a second "active" metal is seen as a useful way to achieve this goal. Mn (5) and Cr (6) significantly enhance the activity of Pd in the NO elimination. In the first case, either dual Pd–Mn or MnO_x entities are believed to facilitate NO dissociation while in the second case, the presence of a Pd–Cr alloy phase, which strongly perturbs the Pd electronic properties, is thought to be the origin of the enhanced NO dissociation. Theoretical studies have shown that Cu can strongly modify the Pd valence state by injecting charge into the *sp* subband (7). The consequence of this electronic modification is that Pd–Cu alloys facilitate NO dissociation with respect to Pd by varying the nature of the NO interaction with Pd surface centers, which change from almost purely covalent (in the case of the pure metal) to a mixture with an ionic component. This ionic component increases with the copper content of the alloy and progressively weakens the N–O bond (8). These theoretical studies suggest that Pd–Cu catalysts might be a potential alternative for future TWC systems. Here copper-rich Pd–Cu systems supported on a conventional, mixed ceria/alumina support have been studied along with a reference monometallic Pd and a binary Pd–Cu reference supported on neat alumina. The $CO + NO + O_2$ reaction has been used as a catalytic test to analyze the behavior of these catalysts under stoichiometric conditions. Characterization under reaction conditions was performed using infrared spectroscopy (DRIFTS), and the specific role of the oxygen vacancies of the oxidic components was studied by electron paramagnetic resonance (EPR). The study attempts a detailed analysis of how the metal–support interaction affects the reactivity of the reactant gas molecules and how electronic and/or geometric modification of Pd by alloying influence these phenomena.

II. EXPERIMENTAL

The CeO_x/Al_2O_3 support was prepared by incipient wetness impregnation of alumina (Condea Puralox, $S_{BET} =$

[1] To whom correspondence should be addressed. E-mail: mfernández@icp.csic.es.

0021-9517/00 $35.00

180 $m^2 g^{-1}$) with an aqueous solution of $Ce(NO_3)_4 \cdot 6H_2O$, corresponding to 10 wt% CeO_2. After drying at 353 K, the support was calcined at 773 K for 6 h in dry air. This support, 10CA, and the parent alumina, A, were impregnated with aqueous $Pd(NO_3)_2 \cdot xH_2O$ and $Cu(NO)_2 \cdot 2H_2O$ to give 0.5 and 1.0 wt% metal loadings, respectively. A monometallic 0.5 wt% Pd10CA reference catalyst was also prepared following a similar procedure. Catalysts were calcined following the same drying/calcination cycle.

Catalytic tests using a 1% CO + 0.1% NO + 0.45% O_2 (N_2 balance) mixture at 30,000 h^{-1} were performed in a Pyrex glass reactor system. Gases were regulated with mass flow controllers and analyzed on line using a Perkin–Elmer 1725X FTIR spectrometer coupled with a multiple reflection transmission cell (Infrared Analysis Inc.). Oxygen concentrations were determined using a paramagnetic analyzer (Servomex 540A). Prior to catalytic testing, *in situ* calcination at 773 K was performed, followed by cooling in synthetic air and a N_2 purge at room temperature (RT). A characteristic test consisted of increasing the temperature from 298 to 823 K at 5 $K \cdot min^{-1}$.

TEM experiments were carried out using a JEOL 2000 FX (0.31 nm point resolution) equipped with a LINK (AN 10000) probe for EDS analysis. Portions of samples were crushed in an agate mortar and suspended in cyclohexene. After ultrasonic dispersion, a droplet was deposited on a nickel grid supporting a perforated carbon film. Micrographs and electron diffractograms were recorded over selected areas with compositions previously characterized by EDS. Diffraction images were digitalized with a scanner and subjected to computer densitometry using in-house software to yield angle-integrated radial profiles.

DRIFTS analysis of adsorbed species present on the catalyst surface under reaction conditions was performed using a Perkin–Elmer 1750 FTIR fitted with an MCT detector. Analysis of the NO conversion at the outlet of the IR chamber was performed by chemiluminescence (Thermo Environmental Instruments 42C). The DRIFTS cell (Harrick) was fitted with CaF_2 windows and a heating cartridge that allowed samples to be heated to 773 K. Samples of ca. 80 mg were calcined *in situ* (as before) and then cooled to 298 K in synthetic air before introducing the reaction mixture and heating at 5 $K \cdot min^{-1}$ to 673 K, recording one spectrum (4 cm^{-1} resolution) every 15 K. The gas mixture (1% CO, 0.1% NO, 0.45% O_2, N_2 balance) was prepared using a computer-controlled gas-blender with 75 $cm^3 \cdot min^{-1}$ passing through the catalyst bed.

EPR spectra were recorded at 77 K with a Bruker ER 200 D spectrometer operating in the X-band and calibrated with a DPPH standard ($g = 2.0036$). Portions of ca. 40 mg were placed inside a quartz probe cell with greaseless stopcocks. A conventional dynamic high-vacuum line was used for different treatments. *In situ* pretreated samples (as before) were reduced with 100 Torr of CO at increasing temperatures (298, 373, 423, and 473 K) for 1 h and evacuated for 30 min at the same temperature. In a parallel set of experiments, after CO treatment and subsequent outgassing at 423 K, NO adsorption (10 Torr) was performed at the same temperature as the CO reduction for 1 h, followed by thorough outgassing. Over these two sets of preconditioned surfaces, oxygen (70 $\mu mol \cdot g^{-1}$ unless otherwise specified) adsorption at 77 K, followed by 30 min outgassing (residual pressure 2×10^{-4} mbar) was performed and oxygen-related radicals were detected by EPR. Some experiments were continued by warming the sample to RT and adsorbing successive doses of oxygen at 77 K.

III. RESULTS

Reaction Tests

The CO and NO conversion profiles obtained for the three catalysts, Pd-Cu/CA, Pd-Cu/A, and Pd/CA, are presented in Fig. 1. Low-temperature ($T < 400$ K) conversion of NO corresponds to adsorption/desorption processes in all cases. The Ce-free sample shows very similar light-off behavior for CO and NO at ca. 500 K. The addition of ceria to the binary Pd–Cu system decreases the CO light-off temperature by more than 100 K while the corresponding modification to the NO light-off was around 75 K. In the presence of ceria, CO oxidation is enhanced to a greater extent than NO reduction while for alumina-supported systems both reactions occur simultaneously.

Addition of copper to a Pd/CA specimen also induces beneficial effects in terms of both CO and NO conversion. CO undergoes ca. 25 K decrease in light-off while the NO profile changes in a more dramatic manner. Below 400 K, both Pd–Cu/CA and Pd/CA catalysts retain NO without N_2 evolution, resulting in similar profiles over the intermediate temperature range. The differences appear in the high

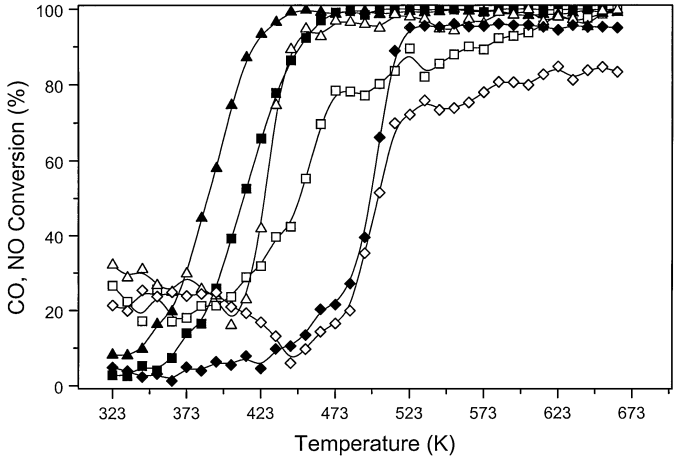

FIG. 1. CO and NO conversion profiles for the CO + NO + O_2 reaction over palladium–copper samples. Triangles, Pd–Cu/CA; squares, Pd/CA; rhombs, Pd–Cu/A. Closed symbols, CO conversion; open symbols, NO conversion.

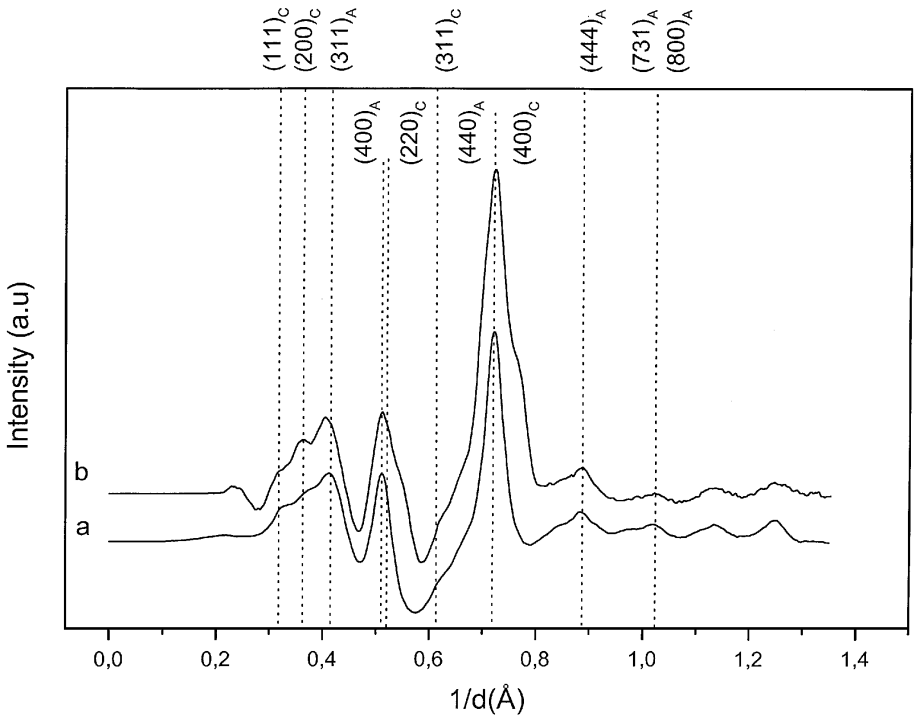

FIG. 2. Radial, angle-integrated densitometry patterns of the electron diffraction rings observed for Pd–Cu/CA before (a) and after (b) reaction. Vertical dashed lines mark the strongest reflections of ceria and alumina (subindexed as C and A, respectively).

conversion region with the presence of copper reducing the 100% conversion temperature by 125 K. The monometallic Cu reference catalyst only shows contribution to NO conversion (data not shown) above 543 K.

Morphological Characterization

As can be seen in Fig. 2, the electron diffraction analysis of calcined and used Pd–Cu materials only gave rings due to ceria (CeO_2) and alumina (Al_2O_3) components. No evidence for Cu- or Pd-containing phases was detected by electron diffraction or EDS, consistent with previous results for Pd/CA (3). We assume that particles above 10 Å should have been detected by diffraction, and this result indicates the high initial dispersion of the active components and the absence of significant sintering during reaction. In Pd–Cu/CA, ceria is (reasonably) homogeneously dispersed, with no significant differences being observed compared with the CA support in the range of Ce/Al atomic ratios (0.02–0.10) obtained by EDS (9).

IR Experiments

DRIFTS recorded under reaction conditions (Fig. 3A–C) indicate for all samples a progressive decrease in CO gas contributions (2175/2125 cm^{-1}) as a function of increasing temperature which roughly parallels the light-off data presented in Fig. 1. The CO_2 gas phase contribution (not shown) did not give the same smooth increase in intensity as a function of CO conversion, partially due to changes in gas phase concentration originating within the beam path but outwith the DRIFTS cell and, possibly, also due to nonlinearity at the relatively high absorption of CO_2 gas within the DRIFT cell due to a combination of the high concentration (at high conversion) and the relatively long path length within the cell. Despite this high absorption at ca. 2350 cm^{-1}, significant baseline distortion was not apparent and bands in the range up to ca. 2270 cm^{-1} could be readily detected. Unlike the CO gas contribution, gas phase NO (centered at 1876 cm^{-1}) was not detected (Fig. 3) as a result of the ten times lower concentration of the latter and its lower absorption coefficient. The most intense features common to all samples are bands at 2231 and 2256 cm^{-1}, ascribed to NCO species adsorbed at exposed octahedral and tetrahedral Al^{3+} cations of the alumina support (10). This species may be a reactive intermediate in the reaction mechanism, as it rapidly disappeared when the NO flow was stopped at low conversion levels and reappear when it was re-introduced. Additional similarities among samples studied include the absence of peaks due to either adsorbed NO species on metallic Pd (1750–1550 cm^{-1}) or adsorbed/gaseous N_2O (ν_{N-N} around 2240 and ν_{N-O} around 1300–1250 cm^{-1}) (12).

For the bimetallic samples, bands due to carbonyls adsorbed on Cu^{2+} (2145 cm^{-1}) and Cu^{+} (2120 and 2100 cm^{-1}) (12), and to nitrosyls on Cu^{2+} (1905, 1865 cm^{-1}) (13) were visible after contact with the reaction mixture at RT. Around 333 K, an additional band at 2136 cm^{-1}, probably due to CO adsorption at Cu^{+} sites (12), was also detected.

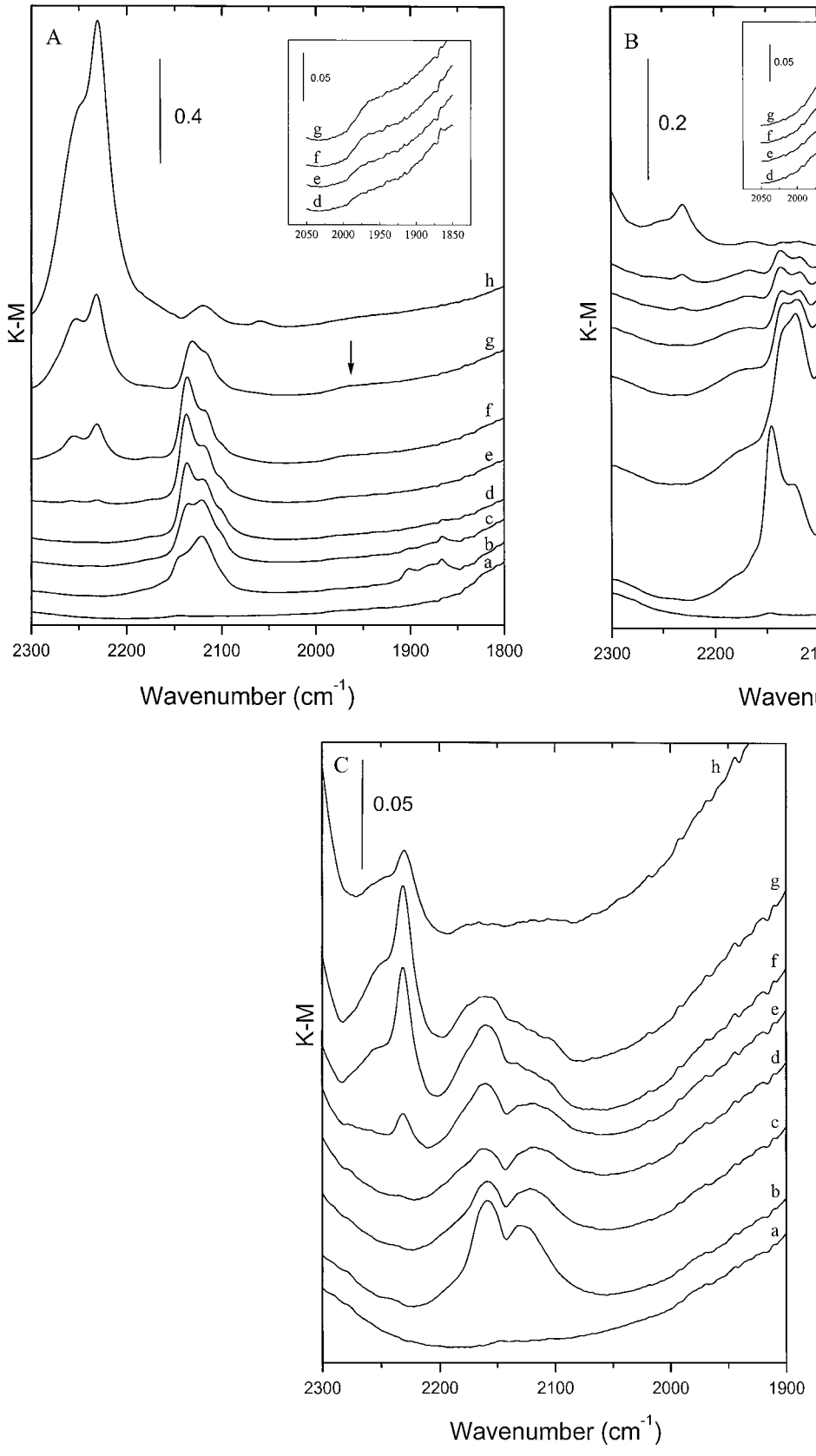

FIG. 3. (A) IR spectra of Pd–Cu/CA sample in a flow of (a) 0.5% of O_2 at 303 K, then 1% CO, 0.1% NO, 0.5% O_2, N_2 balance at (b) 303 K; (c) 333 K; (d) 363 K; (e) 393 K; (f) 423 K; (g) 453 K; and (h) 503 K. An arrow marks the zone displayed in the inset. (B) IR spectra of Pd–Cu/A sample in a flow of (a) 0.5% of O_2 at 303 K, then 1% CO, 0.1% NO, 0.5% O_2, N_2 balance at (b) 303 K; (c) 333 K; (d) 363 K; (e) 393 K; (f) 423 K; (g) 453 K; and (h) 503 K. An arrow marks the zone displayed in the inset. (C) IR spectra of Pd/CA sample in a flow of (a) 0.5% of O_2 at 303 K, then 1% CO, 0.1% NO, 0.5% O_2, N_2 balance at (b) 303 K; (c) 333 K; (d) 363 K; (e) 393 K; (f) 423 K; (g) 453 K; and (h) 503 K.

On heating, the weaker CO–Cu^{2+} and NO–Cu^{2+} bonding interactions allowed desorption of the adsorbates below 373 K, while the CO–Cu^{+} bands, which experienced a downward shift of less than 15 cm^{-1}, were observed over the whole temperature range studied, although they disappeared more quickly in the Pd-Cu/A specimen due, probably, to a stronger sintering process. Note that the high stability at elevated temperatures of the species giving the 2100 cm^{-1} band strongly support an assignment (dubious on the exclusive basis of the frequency) to a CO–Cu^{+} species, excluding the presence of metallic copper. Above 373 K, an additional contribution at ca. 1960 cm^{-1}, due to carbonyls bridging two Pd(0) atoms (14), was detected (Fig. 3 inset). This band was observed at lower temperatures and with a greater intensity for the cerium-containing bimetallic sample. For Pd–Cu/CA, a band at 2060 cm^{-1} was observed from 473 K. This may be attributed to strongly adsorbed on-top carbonyls at Pd(0) atoms, the low frequency resulting from the low coverage and limited dipole coupling between adsorbed molecules at reaction temperatures (14, 15). The dilution of surface Pd centers by Cu (8) or, less likely (for energetic reasons), the presence of Pd in coordinatively unsaturated positions due to small particle size might also contribute to the low-frequency position observed (14–18). The presence of this contribution also suggests that the band at 2100 cm^{-1}, assigned above to CO–Cu^{+}, may also contain a contribution from CO adsorbed at Pd single sites at temperatures between the inital observation of Pd and 473 K (temperature of appearance of the 2060 cm^{-1} band).

The monometallic Pd/CA sample shows significant differences from the Pd-Cu catalysts. No features indicative of adsorption on metallic Pd were detected and new, low-intensity bands around 2160/2120 cm^{-1} were observed below 473 K. These bands may be assigned to Pd^{2+}/Pd^{+} (16) or $Ce^{\delta+}$ ($\delta \leq 3$) species (3, 17, 18), although their absence for the CA support reduced with CO up to 523 K in the absence of Pd, favors the former assignment. The 2160 cm^{-1} band intensity decreases with temperature til NCO species appear (i.e., NO reduction starts), becoming after then a strong feature of the spectra. NCO species were detected as mentioned but with much lower intensity than in bimetallic samples.

After running the CO + NO + O_2 reaction to 523 K (and 473 K for cerium-containing systems in a separate set of experiments), flushing for 15 min and cooling to RT in nitrogen, 100 Torr of CO were admitted at RT and gave rise to maxima in the 2150–1900 cm^{-1} region for all three catalysts (Fig. 4). These IR bands may be considered as indicative of the oxidation state of palladium and copper at high levels of conversion. The monometallic Pd system contains contributions around 2090 and 1970 cm^{-1} due to mono- and bi-coordinated carbonyls adsorbed on close-packed (111)-like and (100)-like metallic facets, respectively (14). The intensity of these bands, particularly of the second one, appear to be strongly depleted in the binary catalysts, which

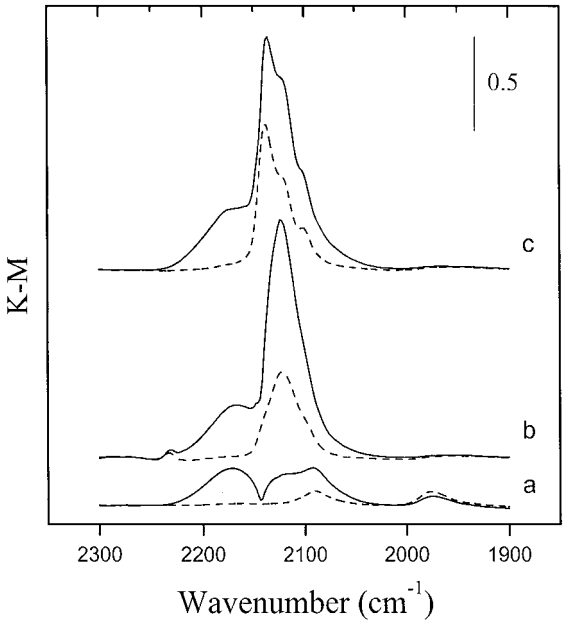

FIG. 4. IR spectra after CO adsorption at RT on spent catalysts. (a) Pd/CA; (b) Pd–Cu/CA; and (c) Pd–Cu/A. Dashed line, 0.1 Torr; full line, 100 Torr.

show additional, intense maxima at around 2100 (CO–Cu^{+} and possibly CO–Pd(0)), 2120 (CO–Cu^{+}), and 2140 (CO–Cu^{2+}) cm^{-1} (12).

EPR Experiments

The EPR results obtained after oxygen adsorption on CO or CO plus NO pre-treated samples are summarized in Fig. 5. For spectra 5Ac and 5Ad, subtraction of the spectra

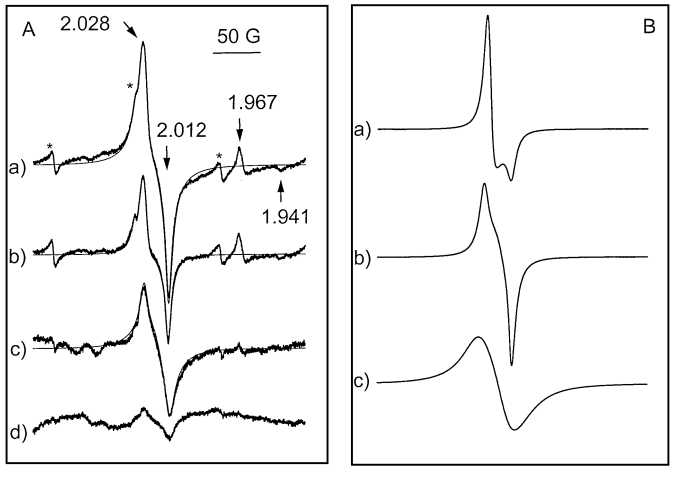

FIG. 5. (A) EPR spectra following oxygen adsorption at 77 K. (a) Sample Pd/CA treated in CO (+ vacuum) at 423 K. (b) Sample Pd/10CA treated in CO (+ vacuum) and subsequently in NO at 423 K. Spectra c and d are similar to spectra a and b, respectively, for sample Pd–Cu/CA. Computer simulations of a–c are overlapped as thinner lines. (B) Typical individual signals used for the simulations of the experimental spectra: (a) O1; (b) O2; and (c) O3.

obtained prior to oxygen adsorption was performed in an attempt to eliminate Cu^{2+} signal contributions. Mn^{2+} impurities were also detected and are indicated by asterisks. As shown in previous studies (19–22), oxygen adsorption on ceria-containing reduced samples leads to formation of superoxide species (Ce^{4+}–O_2^-) due to electron transfer from the surface in a process that can be envisaged (using formal charges) as Ce^{3+}–$V_0 + O_2 \rightarrow Ce^{4+}$–$O_2^-$, where V_0 denotes a doubly charged oxygen vacancy. Evaluation of the intensity and nature of the species formed by this process gives information on the degree of reduction achieved by the sample and on the nature of reduced centres involved in such processes. A signal at $g_\perp = 1.967$ and $g_{||} = 1.941$, corresponding to ceria-related structural defects but not participating in the redox processes due to their relatively high stability (19), was observed in all spectra.

Spectra were analyzed by computer simulations in order to determine the characteristics of the signals obtained. Reasonable simulations could be obtained in the three cases analyzed by considering a single orthorhombic signal at $g_z = 2.028$, $g_x = 2.018$, and $g_y = 2.012$ in each of the cases (Fig. 5Aa–5Ac; no attempt to simulate the spectrum of Fig. 5Ad was carried out due to the low intensity and poor quality of the spectrum obtained). However, in order to obtain an accurate simulation of the central part of the spectra, rather large linewidth values are required for the g_x component (ca. three times higher than those employed for the other two); this differs from previous results for similar samples in which different signals were observed which could be isolated by subjecting the systems to different thermal conditions (4, 19, 20). Also, no simultaneous proper fitting of the tails of the spectra at lower and higher magnetic fields, and of the spectral shapes at magnetic fields corresponding to g_z and g_y values could be achieved by considering single-signal simulations. This strongly suggests that the spectra are formed by overlapping of different signals. It is also worth noting that previous studies on samples with similar characteristics showed spectra containing overlapping signals for samples treated under similar conditions as employed here (3, 4, 9, 21).

In particular, the CA support produced in similar conditions signals called O1 and O2 with parameters ($g_\perp = 2.027$ and $g_{||} = 2.012$) and ($g_z = 2.027$, $g_y = 2.017$, and $g_y = 2.011$), respectively (3, 4, 9, 21). On this basis, simulations of the spectra of Fig. 5 were performed using the mentioned signals O1 and O2. In addition to these signals, the presence of signal O3 was observed which presented a significantly greater line width, and which was required in some cases for proper fitting of the tails at lower and higher magnetic fields. O3 presents a nearly symmetric line shape; fairly good simulations could be obtained when parameters close to those of signal O1 were used, but the best fits were achieved with the parameters $g_z = 2.032$, $g_x = 2.016$–2.015, and $g_y = 2.012$. Table 1 lists the amount of each component used in simulating the EPR spectra. Although the precision of the percentage values is only modest, they allow a semiquantitative evaluation of the differences between samples.

TABLE 1

Characteristics of the EPR Spectra Observed after Oxygen Adsorption at 77 K on the Samples Treated in CO (+ Vacuum) or in CO (+ Vacuum) and Subsequently in NO (+ Vacuum) at 423 K

Sample and treatment	Intensity ($10^1\ \mu mol \cdot g^{-1}$)	Percentage of each signal[a]		
		O1	O2	O3
Pd/CA, CO	2.17	16	51	33
Pd/CA, CO + NO	0.88	36	64	—
Pd–Cu/CA, CO	1.18	—	53	47
Pd–Cu/CA, CO + NO	n.e.[b]	n.e.	n.e.	n.e.

[a] As determined by computer simulations.
[b] n.e. = not evaluated (see text).

The assignments of these O-type signals are based on previous studies (4, 19–22). Signal O1 is attributed to Ce^{4+}–O_2^- species formed at the periphery of two-dimensional cerium oxide patches (2D-Ce entities) dispersed on the γ-Al_2O_3 samples. These cerium oxide species appear to constitute a dispersed form of ceria in these alumina-supported samples, as suggested by previous investigations (21) and confirmed more recently (9). Signal O2 is due to similar Ce^{4+}–O_2^- species located in this case at surface positions of the 2D-Ce patches (9). The proximity of the g values used to simulate signal O3 to those typically observed for Ce^{4+}–O_2^- signals indicates that signal O3 is also due to these species. A signal showing characteristics similar to those of signal O3 has been recently observed for palladium supported on different CeO_2/Al_2O_3 samples and on pure CeO_2, and was attributed to Ce^{4+}–O_2^- species formed at palladium–ceria interfaces of 3D-Ce particles. Such an assignment was based mainly on the promoting effect of palladium on the formation of the corresponding reduced cerium centers (3).

Table 1 provides evidence of the lower amount of Ce^{4+}–O_2^- species produced after CO reduction in the presence of copper. This affects mainly signal O1, as previously observed for monometallic Cu systems, and is attributed to a blocking effect of the metal on surface ionic sites located at the periphery of 2D-Ce patches (22). Most significant in Fig. 5 (and Table 1) is, however, that the treatment with NO at 423 K (subsequent to CO reduction) decreases the number of ceria vacancies and that this decrease is proportionally much more important on the copper-containing sample.

IV. DISCUSSION

Monometallic Catalyst

The Pd/CA sample converts CO from ca. 350 K but only begins to show appreciable NO conversion above 423 K.

CO oxidation using O_2 has been studied recently for this catalyst (3). Fernández-García *et al.* (3) and Xu *et al.* (23) have shown that the presence of metallic Pd is essential for CO activation as only this state of palladium is able to introduce electronic charge in to the $2\pi^*$ anti-bonding orbital, thus weakening the C–O bond (24). Metal–ceria interactions decrease the temperature from which the required metallic state is present under reaction conditions in CO/O_2. In the case of Pd, this state appears from RT (3).

As shown by the absence of the 1970–1960 cm^{-1} band for Pd/CA (Fig. 3C), the presence of NO in the reaction blend maintains Pd in an oxidized state, which appears to be confined to the surface. This deduction is based on the CO adsorption experiments using the used catalyst where only sites indicative of metallic particle surfaces were detected (Fig. 4a). Global reduction of the active phase with surface oxidation has been reported for Pd/Al_2O_3 under CO + NO (25, 26). The detection of NCO (Fig. 3A–3C) for all samples shows, on the other hand, that NO dissociation takes place over these Pd catalysts, independent of the presence/absence of copper. Therefore, some small fraction of reduced Pd, necessary for that reaction step, must exist under reaction conditions.

NO also influences the number and distribution of anionic vacancies on ceria under reaction conditions. As indicated by EPR (Table 1), NO competes with O_2 for vacancies involved in the activation/dissociation of these molecules. As for oxygen (3), for NO O1-type vacancies act as spectators under reaction conditions while the remaining O-type vacancies are active, O3 being the most active. Although the existence of O3 vacancies (clearly detected for pure ceria) is less neatly identified in the 10CA support, the results suggest that anion vacancies formed at the Pd contact with 3D-Ce-like particles are the most effective in promoting the dissociation of both O_2 and NO.

The influence of NO on the Pd and ceria components has important consequences on the light-off behavior of Pd/CA. The reduced number of cerium-anion vacancy centers available for oxygen activation/dissociation due to competition with NO, and the presence of fewer reduced Pd centers which are able to activate CO, lead to the ca. 50 K increase in CO conversion temperature between the $CO + O_2$ (3) and $CO + NO + O_2$ reactions (Fig. 1). This behavior is observed here even for small quantities of NO (1000 ppm) such as those present in exhaust gases under real conditions. The oxidized Pd state, and subsequent limited number of reduced sites, also hinders NO dissociation, which is otherwise only possible at moderate temperatures as a direct result of the presence of ceria. A mechanism by which ceria may enhance NO reduction becomes apparent in the EPR results; anion vacancies at the interface help its dissociation by partially capturing O atoms from NO molecules already activated on the Pd surface.

Bimetallic Catalysts

The first apparent consequence of the addition of Cu to the catalyst formulation is the formation of Pd–Cu alloys under reaction conditions, as deduced from the decreased intensity of the 1970–1960 cm^{-1} band, due to bridging carbonyls on Pd(0) sites (Fig. 4). This decrease cannot be ascribed to a higher dispersion of Pd, as this would give rise to a large increase in the contribution of the 2090 cm^{-1} peak. The absence of bridging sites due to large-scale sintering must be also excluded as TEM did not detect the presence of such Pd particles after reaction. The presence of copper atoms at the surface of the Pd-containing metal particles could explain the decrease in number of Pd(0) neighboring pairs required to produce this adsorbed species. Neglecting effects of dipole–dipole coupling and assuming random mixing of both active components and similar average particle size for all catalysts (as suggested by the microscopy study), a rough estimate of a 0.7 surface copper fraction can be calculated from the intensity loss of the 1970–1960 cm^{-1} band. The lower surface free-energy of copper, the exothermicity of the Pd–Cu alloy formation and the strain effect resulting from the different Pd/Cu atomic radii would suggest that the estimated surface copper fraction is probably a lower limit of the real value (27). On the other hand, a strong dilution of surface Pd centers by Cu has been already observed for Pd/Cu atomic ratios even above unity, depending on the open/closed (packed) surface characteristics (28). Interesting to note is that the ratio between atop and bridge-bonded Pd–CO species (Figs. 3 and 4), so that the ratio between closed and open exposed facets, is different in the bimetallic catalysts studied, suggesting that they may have different alloy particle morphologies. In both specimens, the active metals distribution is completed with the presence of nonalloyed copper species which dominate the 2150–2100 cm^{-1} IR region but are of low significance to interpret the catalytic behavior of the samples.

The first chemical implication of depletion of the surface noble metal with respect to the monometallic reference is the lower number of anionic vacancies detected by EPR in the ceria component (Fig. 5 and Table 1). In the first instance, Cu hinders the formation of catalytically inactive O1-type vacancies. As this happens also for monometallic Cu samples (22), a blocking effect of nonalloyed copper located at the periphery of 2D-Ce particles is the most likely cause of this behavior. Additionally, alloyed copper decreases the number of O2- and O3-type of anion vacancies by about one half and one fourth, respectively (see Table 1). Although these values have at most only semiquantitative significance, they do indicate that the number of all types of vacancies is diminished uppon addition of copper. Combined with the reduced number of active Pd sites available at the surface, these characteristics would be expected to have detrimental consequences on catalytic

activity. However, the overall effect of copper addition is clearly beneficial for both CO and NO conversion (Fig. 1). The detrimental effects are more than compensated by the positive contribution which is derived from the zero-valent state of Pd which is maintained under reaction conditions (1970–1960 cm^{-1} band) as a consequence of the alloying process. Pd-Cu alloys activate CO in a similar manner to Pd, although with reduced adsorption energy (29), but ab initio calculations predict a stronger activation of NO with respect to pure Pd metal as a result of injecting almost one electron into the $2\pi^*$ orbital of the molecule (8). Comparison of PdCu/A and PdCu/CA indicates, however, that the interplay between ceria and the zero-valent alloyed phase is, in fact, the key factor in governing the catalytic activity, as in the case of the monometallic samples in the $CO + O_2$ and $CO + NO + O_2$ reactions (3). This active phase-ceria interaction enhances the formation of the zero-valent phase at lower temperatures (inset of Fig. 3), which facilitates the activation of CO and NO, and provides anion vacancy sites close to that phase which assist in NO and O_2 dissociation at such low temperatures. Although nonalloyed reduced copper in contact with ceria may contribute to the enhanced CO oxidation behavior of the bimetallic catalysts (21), such sites are not active for NO elimination below 543 K. EPR evidence suggests (Fig. 5) that the metal–support interface is, in fact, more effective for NO activation/dissociation when copper is present in the zero-valent phase.

The different surface oxidation state of Pd in mono and bimetallic systems suggests a change in the limiting step of the reaction rate. As observed for Pd/Al_2O_3 (25, 26), this step can be associated with oxygen elimination from the Pd surface ($CO + O_{a,Pd} \rightarrow CO_2$) in the monometallic sample. The metal-adsorbed oxygen is expected to have a higher activation energy for CO_2 formation than the corresponding value for ceria-related oxygen (O^{2-} ions), which is the main source for oxidation processes in the system. For Pd–Cu, the reduced state of the surface indicates that N–O bond dissociation is now the rate-limiting step and, consequently, that O elimination from Pd (CO oxidation on that surface) is significantly favored. The N–O dissociation step is known to be faster than the $CO + O_{a,Pd} \rightarrow CO_2$ step in Pd catalysts (26) and should be faster in the bimetallic than the monometallic catalyst due to the larger activation of the NO molecule produced by its adsorption on Pd–Cu surfaces (8). Both facts constitute the enhancing effect of Cu addition to Pd from a mechanistic point of view.

V. CONCLUSIONS

Ceria plays a key role in CO and NO elimination over monometallic Pd systems. While both reactant molecules are activated over the noble metal component, NO and O_2 dissociation occurs at the metal/ceria interface with the participation of anion vacancies of the lanthanide oxide. Under reaction conditions, Pd remains mostly oxidized at the surface and anionic vacancies located at 3D-Ce particles are believed to be the most effective in promoting the dissociation processes required in the reaction mechanism. The active component–ceria interface also governs the catalytic activity for Pd–Cu systems. However, Cu modifies the noble metal oxidation state during reaction, stabilizing the zero-valent Pd while, on the other hand, reducing the number of otherwise active anion vacancies of the ceria. Both effects are explained by the formation of a Pd–Cu alloy which is most likely surface enriched in Cu, and which is thermodynamically more stable than the separated metals. The two effects from Cu addition have opposing results over the catalytic activity but the net-effect of copper addition to Pd is beneficial. From a mechanistic view, copper improves activity by enhancing the rate of the two elemental steps: CO oxidation on Pd surfaces and N–O dissociation.

ACKNOWLEDGMENTS

M.F.-G. and A.M.-A. gratefully acknowledge the "Ministerio de Educación" of Spain and the "Comunidad de Madrid" for a Postdoctoral contract and grant, respectively. We thank the Royal Society (London) for a European Exchange Fellowship (M.F.-G.) and a University Research Fellowship (J.A.A.). Thanks are also due to Mr. F. Sánchez Constela for performing the EPR experiments. Support from CAICYT (Project MAT 97-0696-CO2-O1) and CAM (Project 06M/084/96) is fully appreciated.

REFERENCES

1. Searles, R. A., *Stud. Surf. Sci. Catal.* **116**, 23 (1998).
2. Trovarelli, A., *Catal. Rev. Sci. Eng.* **38**, 439 (1996).
3. Fernández-García, M., Martínez-Arias, A., Salamanca, N. L., Coronado, J. M., Anderson, J. A., Conesa, J. C., and Soria, J., *J. Catal.* **187**, 474 (1999).
4. Martínez-Arias, A., Coronado, J. M., Cataluña, R., Conesa, J. C., and Soria, J., *J. Phys. Chem. B* **102**, 4357 (1998).
5. Trillat, J. F., Massadier, J., Morawek, B., Praliaud, H., and Renouprez, A. J., *Stud. Surf. Sci. Catal.* **116**, 103 (1998).
6. El Hamdaoui, A., Bergeret, G., Massadier, J., Primet, M., and Renouprez, A. J., *J. Catal.* **148**, 47 (1994).
7. Fernández-García, M., Conesa, J. C., Clotet, A., Ricart, J. M., López, N., and Illas, F., *J. Phys. Chem. B* **102**, 141 (1998).
8. Illas, F., López, N., Clotet, A., Ricart, J. M., Conesa, J. C., and Fernández-García, M., *J. Phys. Chem. B*, **102**, 8017 (1998).
9. Martínez-Arias, A., Fernández-García, M., Salamanca, L. N., Conesa, J. C., and Soria, J., *J. Phys. Chem. B*, in press.
10. Anderson, J. A., Márquez-Alvarez, C., López-Muñoz, M. J., Rodríguez-Ramos, A., and Guerrero-Ruiz, A., *Appl. Catal. B* **14**, 189 (1997).
11. Ramsier, R. D., Gao, Q., Walternung, H. N., Lee, K.-W., Nooij, O. W., Lefferts, L., and Yates, J. T., *Surf. Sci.* **320**, 209 (1994).
12. Martínez-Arias, A., Fernández-García, M., Soria, J., and Conesa, J. C., *J. Catal.* **182**, 367 (1999).
13. Fernández-García, M., Gómez-Rebollo, E., Guerrero-Ruiz, A., Conesa, J. C., and Soria, J., *J. Catal.* **172**, 146 (1997).
14. Hollins, P., *Surf. Sci. Rep.* **16**, 51 (1992).
15. Rochefort, A., and Fournier, R., *J. Phys. Chem.* **100**, 13506 (1996).
16. Bensalem, A., Muller, J. C., Tessier, D., and Buzon-Verduraz, F., *J. Chem. Soc., Faraday Trans.* **92**, 3233 (1996).

17. Skarman, B., Wallenberg, L. R., Larsson, P.-O., Andersson, A., Bovin, J.-O., Jacoben, S. N., and Helmersson, U., *J. Catal.* **181**, 6 (1999).
18. Badri, A., Binet, C., and Lavalley, J. C., *J. Chem. Soc., Faraday Trans.* **92**, 1603 (1996).
19. Martínez-Arias, A., Coronado, J. M., Conesa, J. C., and Soria, J., *in* "Rare Earths" (R. Sáez Puche and P. Caro, Eds.), p. 299. Complutense, Madrid, 1997.
20. Soria, J., Martínez-Arias, A., Coronado, J. M., and Conesa, J. C., *Coll. Surf. A* **115**, 215 (1996).
21. Soria, J., Coronado, J. M., and Conesa, J. C., *J. Chem. Soc., Faraday Trans.* **92**, 1619 (1996).
22. Martínez-Arias, A., Cataluña, R., Conesa, J. C., and Soria, J., *J. Phys. Chem. B* **102**, 809 (1998).
23. Xu, X., and Goodman, D. W., *J. Phys. Chem.* **97**, 7711 (1993).
24. Pacchioni, G., and Bagus, P. S., *J. Chem. Phys.* **93**, 1209 (1990).
25. Almasateer, K., and Chuang, S. S. C., *J. Catal.* **184**, 189 (1999).
26. Pisanu, A. M., and Gigola, D. E., *Appl. Catal. B* **20**, 179 (1999).
27. Ponec, V., and Bond, G. C., "Catalysis by Metals and Alloys," Chap. 8. Elsevier, Amsterdam, 1995.
28. Fernández-García, M., Anderson, J. A., and Haller, G. L., *J. Phys. Chem.* **100**, 16247 (1996) and references therein.
29. Debauge, Y., Abou, M., Bertolini, J. C., Massadier, J., and Rochefort, A., *Appl. Surf. Sci.* **90**, 15 (1995).